

PAPER • OPEN ACCESS

Evaluation of the nonlinear surface resistance of REBCO coated conductors for their use in the FCC-hh beam screen

To cite this article: P Krkoti *et al* 2022 *Supercond. Sci. Technol.* **35** 025015

View the [article online](#) for updates and enhancements.

You may also like

- [Design and performance studies of a hadronic calorimeter for a FCC-hh experiment](#)
J. Faltova
- [Stability limits with Landau damping in the FCC-hh](#)
D. Astapovych, O. Boine-Frankenheim, V. Gubaidulin et al.
- [Design and performance of an electromagnetic calorimeter for a FCC-hh experiment](#)
A. Zaborowska



IOP | ebooks™

Bringing together innovative digital publishing with leading authors from the global scientific community.

Start exploring the collection—download the first chapter of every title for free.

Evaluation of the nonlinear surface resistance of REBCO coated conductors for their use in the FCC-hh beam screen

P Krkotic^{1,2} , A Romanov³, N Tagdulang^{1,2} , G Telles³ , T Puig³, J Gutierrez³ , X Granados³, S Calatroni⁴ , F Perez¹, M Pont^{1,*}  and J M O'Callaghan² 

¹ ALBA Synchrotron Light Source, Carrer de la Llum 2-26, 08290 Cerdanyola del Valles, Barcelona, Spain

² Commsenslab, Department of Signal Theory and Communications, Universitat Politècnica de Catalunya (UPC), C/Jordi Girona 1, 08034 Barcelona, Spain

³ Institut de Ciència de Materials de Barcelona, Campus de la UAB, Carrer dels Til·lers, 08193 Bellaterra, Barcelona, Spain

⁴ CERN Technology Department, Espl. des Particules 1, 1211 Meyrin, Switzerland

E-mail: pont@cells.es

Received 13 October 2021, revised 8 December 2021

Accepted for publication 17 December 2021

Published 7 January 2022



CrossMark

Abstract

To assess the feasibility of using high-temperature superconductors for the beam screens of future circular colliders, we have undertaken a study of the power dependence of the microwave surface resistance in state-of-the-art REBCO coated conductors at about 8 GHz and 50 K. We have employed a dielectric resonator to produce radio-frequency (RF) electromagnetic fields on the surface of the coated conductors having amplitudes similar to those generated by proton bunches circulating in the vacuum chamber of the proposed future circular collider Hadron-Hadron (FCC-hh) at CERN. We show that surface resistances in REBCO coated conductors without artificial pinning centers are more affected by a RF magnetic field than those containing nano-inclusions. Despite that, at 8 GHz, 50 K, and 9 T, most REBCO coated conductors studied outperform copper in terms of surface resistance, with the best sample having a 2.3 mΩ surface resistance while being subject to an RF field 2.5 times stronger than that in the FCC-hh. We also extrapolate the measured data to 16 T and 1 GHz, the actual FCC-hh dipole magnetic field, and the mid-beam frequency spectrum, demonstrating the possibility of lowering the surface resistance of the vacuum chamber by up to two orders of magnitude compared to copper. Further, we discuss the correlation between the time structure of the electromagnetic fields provided by vector network analyzers compared to the proton bunches' time structure in the collider and present the effect of low alternating magnetic fields on vortex displacement and the possibility of demagnetization of superconducting samples.

* Author to whom any correspondence should be addressed.



Original Content from this work may be used under the terms of the [Creative Commons Attribution 4.0 licence](https://creativecommons.org/licenses/by/4.0/). Any further distribution of this work must maintain attribution to the author(s) and the title of the work, journal citation and DOI.

Supplementary material for this article is available [online](#)

Keywords: coated conductors, future circular collider, high-temperature superconductor, surface resistance

(Some figures may appear in colour only in the online journal)

1. Introduction

The future circular Hadron-Hadron collider (FCC-hh) study [1] is an international collaboration hosted by CERN to design the successor of the large Hadron collider (LHC) [2]. The FCC-hh aims to be a Hadron-Hadron collider with a center-of-mass collision energy of 100 TeV in a 100 km long accelerator. To steer the two counter-rotating proton beams at 50 TeV, superconducting bending magnets up to 16 T are required. All these parameters demand an important technological development effort compared to the present LHC, which has a center-of-mass collision energy of 14 TeV, in a 27 km long accelerator that uses bending magnets of 8.3 T to steer the proton beams [2]. Also, the higher beam energy compared to the LHC results in a substantial increase of the emitted synchrotron radiation (SR) that reaches a linear power density of about 35.7 W m^{-1} per beam [3]; a factor 160 larger than in the LHC.

Similar to the LHC, the vacuum pipes for the two counter-rotating beams in the FCC-hh will be incorporated into a standard yoke cooled by superfluid helium at 1.9 K. To limit the beam-induced heat load transfer to the cold bore of the magnets, beam screens (BSs) are introduced in the vacuum pipes to intercept the SR power. Extensive studies [4] have shown that a good compromise between the electrical cooling power required to maintain the cold bores temperature at 1.9 K and the avoidance of exciting vapor pressure instabilities requires keeping the BS between 40 and 60 K. The baseline design of the BS [5] includes a double structure. The first structure is the primary or inner chamber made of P506 stainless steel sheet, 1 mm thick, which is open on the mid-horizontal plane to let the SR pass through and be absorbed in lateral baffles designed explicitly for this purpose. The inner chamber is colaminated with a 0.3 mm thick oxygen-free electronic grade copper (Cu) layer to achieve low impedance values. The second structure is the outer chamber, or ante-chamber, and serves as SR absorber and secondary electron stopper. However, the restriction to operate the BS between 40 and 60 K—much higher temperatures than those of the LHC (5–20 K)—raises the surface impedance presented by the Cu coating to the proton beams. It leads the resistive wall impedance to be the primary driver of transverse beam instabilities in the proposed FCC-hh [6, 7]. Suggestions to look for materials other than Cu were put forward within the FCC-hh collaboration [1].

One such possibility is the use of high-temperature superconductors (HTS) which have transition temperatures above 90 K and surface resistances well below that of copper in the temperature range of interest [8], i.e. between 40 and 60 K. In recent years, several studies have shown the potential of $\text{REBa}_2\text{Cu}_3\text{O}_{7-x}$ coated conductors (REBCO-CCs, RE = Y,

Gd, Eu) as coating materials for the BS in order to minimize the beam impedance [9–18]. Even though these previous works on coated conductors have shown that their small-signal surface resistance is significantly below that of Cu, there are other aspects related to their surface impedance that may compromise their use in the FCC-hh BS, specifically [19–25]: its dependence on radio-frequency (RF) strength under large applied DC magnetic fields, and the appearance of temperature effects, including self-heating, resulting from the application of large RF fields.

This paper aims to experimentally evaluate the nonlinear behavior of REBCO-CC's surface resistance in the presence of a DC magnetic field superimposed on a RF magnetic field strength of varying amplitude, comparable with that of the FCC-hh, and relate the observed behavior to the FCC-hh BS performance. The evaluation is done for commercially available REBCO-CCs coming from six different providers that use different fabrication technologies, as summarized in table 1.

The paper is organized in the following way. Section 2 describes the numerical determination of the RF magnetic field strength at the surface of the coating for the baseline FCC-hh BS design. Section 3 specifies the experimental apparatus for measuring the surface resistance of REBCO-CCs as a function of temperature, applied DC magnetic field and vector network analyzer (VNA) output power. In section 4, the experimental results of surface resistance versus radio-frequency power and DC magnetic field are described and discussed. In section 5, the measurements of transient thermal effects are presented and reviewed. Section 6 is devoted to the concept of flux shaking; the relevant measurements are illustrated and discussed.

2. FCC-hh beam screen RF field

In this section, we calculate the expected azimuthal RF magnetic field strength $H_{\text{RF,FCC}}$ on the surface of the inner FCC-hh BS, which will be used as the reference value for the following experiments. Operating parameters for the FCC-hh have been taken from [1] and are summarized in table 2. The circulating current in the FCC-hh is expected to be 0.5 A. This current is distributed in bunches, each consisting of 10^{11} protons that will induce image currents on the surface of the BS coating. With a root-mean-square (RMS) bunch length of 8 cm [1], the equivalent peak current per bunch is about $I_{p,bunch} = 24 \text{ A}$. To calculate the RF magnetic field strength, the actual shape and dimensions of the BS have been taken from [3]. In this case, $H_{\text{RF,FCC}}$ is calculated using a finite-element method (FEM) solver implemented in Mathematica®.

Table 1. Coated conductor characteristics for different providers. The acronyms for the growth methods are: pulsed laser deposition (PLD), double disordered REBCO layer by PLD (DD-PLD), reactive co-evaporation by deposition and reaction (RCE-DR), metalorganic chemical vapor deposition (MOCVD) and electron-beam physical vapor deposition (EB-PVD) [13].

Provider	Rare-earth in REBCO	Nano-inclusions	HTS-thickness (μm)	Growth method
Bruker	Y	BaZrO ₃	1.6	DD-PLD
Fujikura	Gd	None	1.8	PLD
Fujikura APC*	Eu	BaHfO ₃	2.5	PLD
SuNAM	Gd	None	1.6	RCE-DR
SuperOx	Gd	None	0.9	PLD
SuperPower	Y,Gd	BaZrO ₃	1.5	MOCVD
Theva	Gd	None	3.0	EB-PVD

* Artificial pinning center (APC).

Table 2. FCC-hh relevant baseline parameters [1].

Parameter	FCC-hh
Circumference (km)	97.75
Current (mA)	500
Harmonic number	130 680
RF cavity (MHz)	400.79
Proton bunches	10 400
Protons per bunch	10^{11}
RMS bunch length (cm)	8

Starting with Maxwell's equations and replacing the magnetic field in the stationary Maxwell-Ampere law by the vector potential A in the magneto-static approach, the Poisson equation in the Coulomb gauge can be written as:

$$-\nabla^2 A = -\mu_0 J_{p,bunch}, \quad (1)$$

where $J_{p,bunch} = I_{p,bunch}/\Omega_{BS}$ refers to the peak current density. To solve this equation, it is assumed that a perfect electric conductor (PEC) surrounds the vacuum filled region Ω_{BS} with the boundary conditions:

$$\Gamma_N : \partial A = 0 \quad \text{for } (x,y) \in \partial\Omega_{BS}, \quad (2)$$

$$\Gamma_D : A = 0 \quad \text{for } (x,y) \in \partial\Omega_{BS}, \quad (3)$$

where the subscripts N and D refer to a Neumann and Dirichlet boundary condition, respectively. The solution for the vector potential A is found by numerically solving equation (1) for a fine mesh of the region Ω_{BS} ($\approx 140\,000$ triangular elements) and using A to find the azimuthal magnetic field strength $\mu_0 H_{RF,FCC} = \nabla \times A$ shown in figure 1. The result demonstrates that the inner coating of the BS marked in black facing the protons directly would be exposed to an RF azimuthal magnetic field strength between $H_{RF,FCC} = 130\text{--}230 \text{ A m}^{-1}$ depending on the positioning of the coating, which is much smaller than the first critical magnetic field of REBCO-CCs. Close to the openings of the mid-horizontal plane to let the SR pass, the magnetic field strength is also large although this might be connected to the sharp edge in the models used and might be a numerical artefact of the FEM solver.

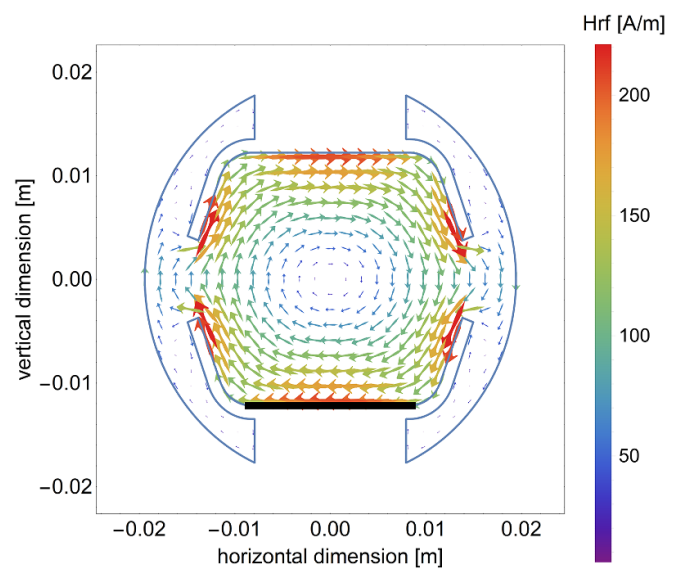


Figure 1. Vector field plot of the azimuthal magnetic field strength distribution produced in the inner part of the FCC-hh beam screen (baseline design).

3. Experimental arrangement

A dielectric resonator (DR) cavity [26, 27] has been used to measure the quality factor Q_0 as a function of applied RF power. Measurements are performed in a Quantum Design PPMS[®] system capable of applying DC magnetic field B_{DC} up to 9 T perpendicular to the samples surface at temperatures between 4.2 and 300 K.

The dielectric resonator used in this study consists of a cylindrical brass cavity loaded with a low-loss ($\tan(\delta) \leq 10^{-4}$) and high-permittivity c -oriented ($\epsilon_r(50 \text{ K}) \approx 110$) rutile (TiO₂) cylinder, shielded axially by the pair of samples under measurement as shown in figure 2. The sample size is 12 mm \times 12 mm since the commercially coated conductors used for this study are available in km lengths with a standard width of 12 mm. The resonator was designed to operate in the TE₀₁₁ mode. This mode is typically used for microwave characterization due to its azimuthal currents, which make resonator parameters (quality factor and resonant frequency) insensitive to

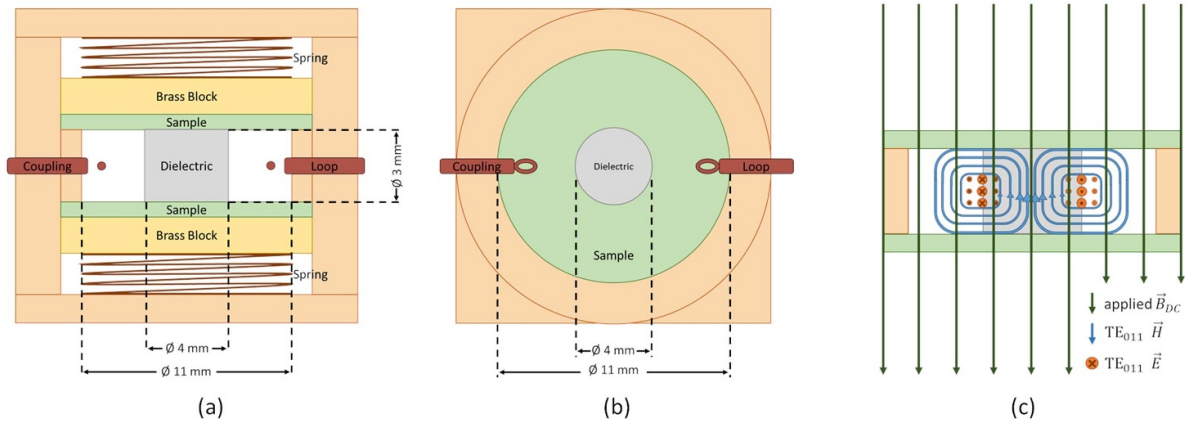


Figure 2. Scheme of the rutile loaded dielectric resonator: (a) side view and (b) top view (c) field distribution in the vertical plane. The REBCO films of both samples face towards the inside of the resonator.

the electrical contact between the samples under test and the lateral walls [28–31]. Given the dimensions of the REBCO-CCs, the radius of the cavity was chosen to be $R = 5.5$ mm. The dimensions of the rutile cylinder (length $L = 3$ mm, diameter $D = 4$ mm) were determined through Computer Simulation Technology Studio Suite® simulations to ensure that the loss of the lateral walls would be negligible compared to other sources of loss and that no other modes would resonate at frequencies close to that of the TE_{011} mode.

To investigate the RF surface magnetic field strength dependency of the surface resistance, it is necessary to specify the relationship between the electromagnetic fields in the DR (equations (S1) and (S2) in the supplementary material (available online at stacks.iop.org/SUST/35/025015/mmedia)) and the VNA output power P_{out} . This can be done by relating the stored energy W , the unloaded quality factor Q_0 , the dissipated power P_{diss} , and the electromagnetic fields inside the resonator, which gives the peak surface RF magnetic field strength H_0 :

$$\begin{aligned} H_0 = H_\rho(\rho_{max}, L) &= m_B(\rho_{max}, L) \sqrt{2\pi f_0 W} \\ &= m_B(\rho_{max}, L) \sqrt{Q_0 P_{diss}}, \end{aligned} \quad (4)$$

where ρ_{max} refers to the radius where the azimuthal surface RF magnetic field strength is maximum and L is the length of the dielectric cylinder. The complete expression of the field factor m_B is given in equation (S7). The resulting RF radial field on the sample ($H_\rho(\rho, L)$) generates azimuthal currents in the pair of samples under measurement with maximum amplitude at $\rho_{max} = 1.3$ mm (figure A1 in supplementary material).

The relationship between Q_0 and surface resistance R_S is given by [32]:

$$\frac{1}{Q_0} = \sum_{i=1}^3 \frac{R_{S_i}}{G_i} + p \cdot \tan \delta, \quad (5)$$

where R_{S_i} , $i = 1, \dots, 3$ are the surface resistances of the upper, lower and lateral walls, and G_i their corresponding geometrical factors. Due to the cavity symmetry, the geometrical factors

of the upper and lower walls are identical. Furthermore, the dimensions of the dielectric are chosen such that the contribution of the lateral wall to the summation in equation (5) is negligible. In that case, the average surface resistance of the two samples under test can be written as:

$$R_S = \frac{G}{2} \left(\frac{1}{Q_0} - p \cdot \tan(\delta) \right), \quad (6)$$

where G is the geometric factor of the upper (or lower) wall and R_S is defined as the average surface resistance of the samples under test. The geometrical factor and filling factor for the cavity used in this study are $G = 212.9 \Omega$ and $p = 0.997$ [33]. The value for the loss tangent $\tan(\delta) = 1.82 \times 10^{-6}$ has been measured by [27]. For the accurate post-processing of the surface resistance, the unloaded quality factor is obtained using an algorithm based on Moore-Penrose inverse routines, including an adaptive outlier removal that discards distorted measurement points to increase the accuracy of the R_S determination [34].

To perform the complex S-parameter measurements at high microwave power, a P5002A Keysight Streamline USB VNA that provides power up to +13 dBm at about 8 GHz has been used. To establish the relation between the output power from the VNA P_{out} and the dissipated power in the cavity P_{diss} , the insertion loss of the cables between the VNA and the resonator has to be quantified. For the test cable outside the cryostat (figure 3), this is a simple measurement that can be performed with a power meter. However, the semi-rigid cable inside the cryostat is not accessible. Its insertion loss is estimated to be half the off-resonance return loss in dB. Accordingly, the available input power P_0 at the resonator is 2.65 dB below the VNA output power (P_{out}). In these conditions, the P_{diss} in the resonator can be related to P_0 through the coupling factors β_1, β_2 [35]:

$$P_{diss} = P_0 \frac{4 \beta_1}{(1 + \beta_1 + \beta_2)^2}. \quad (7)$$

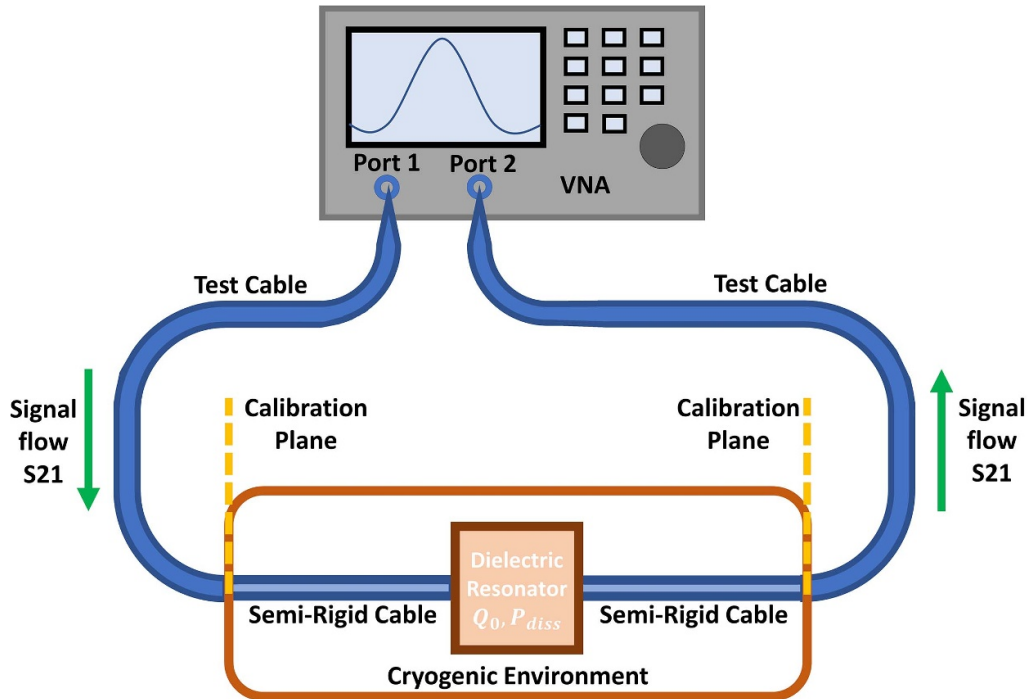


Figure 3. Layout of the experimental setup.

Once the power dissipated in the sample and the quality factor are known, we can determine the amplitude of the fields in the cavity through equation (4).

A set of seven commercially available REBCO-CC samples differing from their architecture and microstructure has been used for this study. The coated conductors have been provided by Bruker HTS GmbH, Fujikura Ltd SuNAM CO Ltd SuperOx, SuperPower Inc. and Theva Dünnschichttechnik GmbH. Coated conductors were provided without the usual silver/copper stabilizer jacket. However, the protective silver layers had to be etched away from the samples provided by Fujikura and SuperOx. The removal process of the silver-layer has been done using a solution 1:1:5 of $\text{NH}_3:\text{H}_2\text{O}_2:\text{CH}_3\text{OH}$.

To be consistent with the FCC-hh most probable cool down procedure, the measurements with the PPMS system were performed by zero-field cooling the samples down to 50 K where the temperature was stabilized before applying the DC magnetic field B_{DC} . Microwave measurements were carried out by applying the VNA output power P_{out} from -40 dBm up to $+10$ dBm in 5 dB steps, and in addition, one measurement at the maximum output power of $+13$ dBm. The power sweep was performed for DC magnetic field from 0 to 9 T in 1 T steps without changing the temperature in between the magnetic sweep measurements. Furthermore, at $B_{DC} = 1$ T and $B_{DC} = 9$ T, measurements were performed as a function of the VNA sweep time to study possible transient thermal effects. Finally, the REBCO-CCs were magnetized to 9 T and a final power sweep without DC magnetic field was performed to determine the extension of any flux shaking mechanism. The VNA was set with 401 frequency points and an intermediate frequency (IF) bandwidth of 10 kHz leading to a sweep time of 3.9 ms. The frequency sweep was set to be centered at

the resonance frequency with a span factor ten times the 3 dB bandwidth.

4. Surface resistance vs RF power and DC field

Surface resistance R_S as a function of VNA output power P_{out} and DC magnetic field B_{DC} for one of the providers (Theva) can be seen in figure 4. Figure 4(a) shows a nonlinear behavior of the surface resistance as it increases with a power-law dependence for VNA output power levels above -10 dBm. Figure 4(b) shows the magnetic field dependence of R_S at different VNA output powers. Two main features are observed: R_S increases with the DC magnetic field starting from non-zero values at zero magnetic field, and the higher the VNA output power, the higher the surface resistance. Generally, three terms describe the total surface resistance [9]. First, a contribution is resulting from the BCS-theory that depends on the gap parameter of the superconductor. Second, lattice defects, grain boundaries, or impurities are summarized as the residual resistance. These two terms depend on the strength of the RF field applied on the samples (and hence on the VNA output power) but do not depend on the applied DC magnetic field and are the dominating terms at $B_{DC} = 0$. Finally, the only applied DC magnetic field dependent term accounts for the creation of vortices in the superconductor and their dissipative oscillating movement around their pinning centers when driven by an RF current [18]. This last term is the dominating one at high magnetic fields and in the work presented here. Additionally, other mechanisms may also partially contribute to the nonlinear surface resistance observed in figure 4: RF flux line dynamics, including nucleation-, self-heating and intrinsic pair breaking

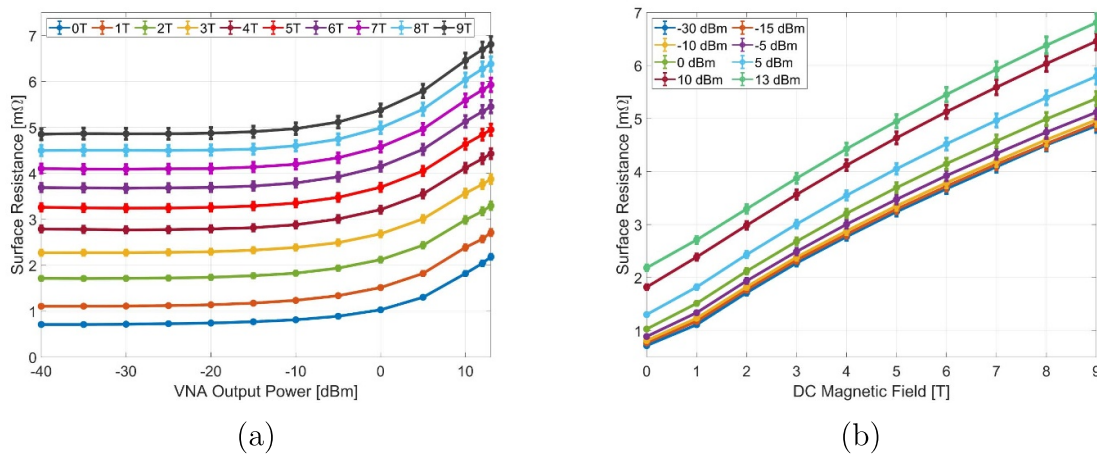


Figure 4. Surface resistance at 8 GHz and 50 K as a function of VNA output power for several DC magnetic fields. Data is shown for Theva.

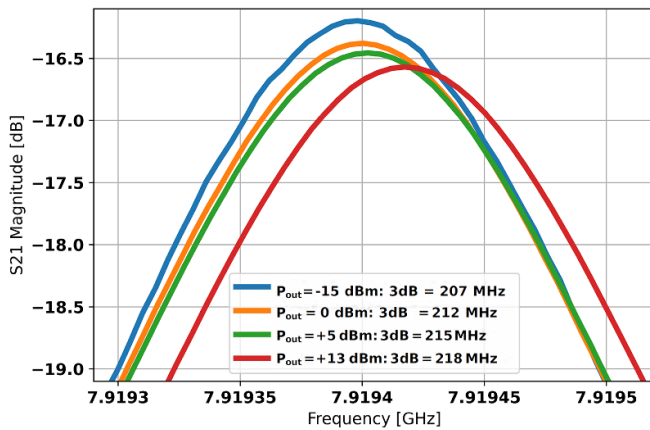


Figure 5. Measured transmission coefficient S_{21} within 3 dB bandwidth for a single resonant mode without DC magnetic field and different VNA output power. The first value in the legend refers to the output power of the VNA and the second value refers to the 3 dB bandwidth value. Data is shown for SuperOx.

[8, 19, 36]. We rule out any significant contribution to R_S from the substrate under the superconducting layer. While this may happen in some thin films, our previous work shows that this contribution is generally negligible in most REBCO coated conductors [16].

Figure 5 illustrates how a surface impedance dependent on RF power affects the S_{21} parameter for the specific case of the SuperOx sample. The S_{21} is the transmission coefficient defined as the ratio of an outgoing travelling wave at port 2 to an incoming travelling wave at port 1 [37]. The higher the VNA power, the broader the resonant peak, which is indicated in the legend of figure 5 by the 3 dB bandwidth value. The higher the bandwidth the lower the resulting quality factor due to a higher R_S . As shown in the same figure, VNA power P_{out} also causes a shift of the resonance frequency caused by the dependence of surface reactance on RF field amplitude. Similar results have been obtained for the other samples used in this work.

Figure 6 shows the RF peak surface magnetic field strength H_0 and surface resistance R_S as a function of B_{DC} for $P_0 = +13$ dBm. The green area marks the expected RF azimuthal magnetic field strength $H_{RF,FCC}$ at the surface of the FCC-hh BS following the calculations shown in figure 1. The results shown in figure 6(a) are for REBCO-CCs that contain nano-inclusions as artificial pinning centers (APC), as indicated in table 1. The lower R_S in REBCO-CCs with APC generates RF field strengths on the samples (H_0) larger than those in samples without APC (figure 6(b)). When compared to the RF field estimated for the FCC-hh ($H_{RF,FCC}$), all samples with APC were within or above the $H_{RF,FCC}$ estimation, and most of the samples without APC were within this estimate too.

Table 3 lists the peak RF magnetic field strength applied on each sample compared to the RF azimuthal magnetic field in the FCC-hh and compared to the RF field used in previous studies. Note that peak RF fields in all samples are much larger than the ones reported in our previous studies [13, 16] and comparable or larger than the RF azimuthal field in the FCC-hh.

Results for the Theva sample deserve a specific discussion. This sample showed the most significant increase in R_S and drop on H_0 with respect to its zero-field ($B_{DC} = 0$ T) values, probably due to the inclined growth technology used. The c -axis of this REBCO tape is tilted by approximately 30 degrees with respect to the substrate normal, transversely to the tape length [13]. Hence, the magnetic field is not directed along the REBCO c -axis, leading to an effective applied DC magnetic field of $0.9B_{DC}$, as discussed in detail in [13]. Further, the circulating currents induced into the sample due to H_0 have to flow partially in the growth direction but also perpendicularly to it. Theva's growth technology seems to raise the surface resistance close to that of FCC-hh copper at 9 T. This is significantly larger than our previous results in [13]. Still, it has to be stated that in the FCC-hh, the image currents would flow only parallel to the growth direction.

Due to experimental limitations, our measurements have been performed at higher frequencies (8 GHz) and lower DC magnetic field (9 T) than those specified for the FCC-hh (up

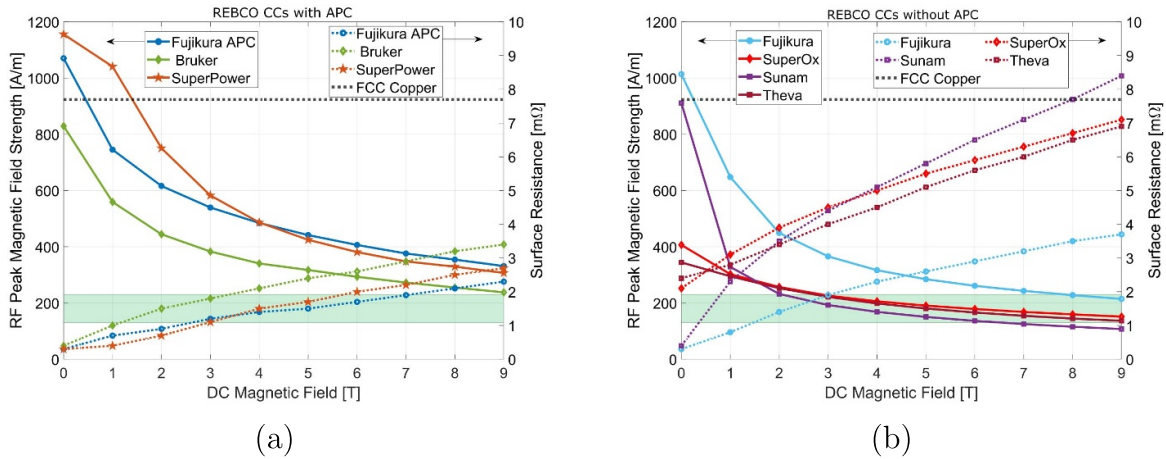


Figure 6. RF peak surface magnetic field H_0 and surface resistance vs. DC magnetic field at 8 GHz and 50 K for REBCO-CCs with and without artificial pinning centers for the maximum input power of +13 dBm we have studied. Solid lines show the RF surface peak magnetic field strength (left axes) on the samples while the dashed lines show their surface resistance (right axes). The green area indicates the azimuthal RF magnetic field strength $H_{RF,FCC}$, to be found in the FCC-hh BS as calculated in section 2. The horizontal arrows indicate the vertical axis to which each legend belongs. The black dashed line indicates the surface resistance of FCC-hh copper for comparison. The measured magnetoresistive effect on copper is negligible small at 50 K, hence the 0 T value is presented.

Table 3. RF peak surface magnetic field strength ratios for the studied providers. The ratios are defined as follows: first column: RF surface magnetic field strength at maximum output power +13 dBm over RF surface magnetic field strength at -15 dBm at 9 T and second column: RF surface magnetic field strength at maximum output power +13 dBm over the lower and upper RF azimuthal magnetic field strength values for FCC-hh also at 9 T.

REBCO-CC	$\frac{H_0(+13 \text{ dBm})}{H_0(-15 \text{ dBm})}$	$\frac{H_0(+13 \text{ dBm})}{H_{RF,FCC}}$
Bruker	25.2	1.8–1.0
Fujikura APC	24.9	2.5–1.4
SuperPower	25.1	2.4–1.3
Fujikura	25.7	1.7–0.9
SuNAM	25.8	0.8–0.5
SuperOx	25.0	1.2–0.7
Theva	18.5	1.1–0.6

to 1 GHz and 16 T, respectively). It shall be mentioned that in the present experiments, B_{DC} is always perpendicular to the REBCO-CC surface—the worst case in terms of surface resistance [38]—while in the FCC-hh BS, coated conductors will have different orientations with respect to the magnetic field. In the paragraphs below, we extend the results to $f = 1$ GHz and $B_{DC} = 16$ T to match the worst-case FCC-hh conditions.

As shown in figure 6, above $B_{DC} = 2$ T all samples show a nearly linear increase of R_S with the applied DC magnetic field, indicating that RF losses are proportional to the areal density of vortices, which is consistent with many theoretical calculations [11]. Accordingly, we have fitted our surface resistance vs. DC field dependence with a linear dependence above 4 T where a clear linear dependence is visible, including an independent term $R_S = mB_{DC} + n$. In this equation, the proportional term m takes into account the flux-flow and pinning contribution to the surface resistance [11], while the independent term n accounts for the field-independent residual

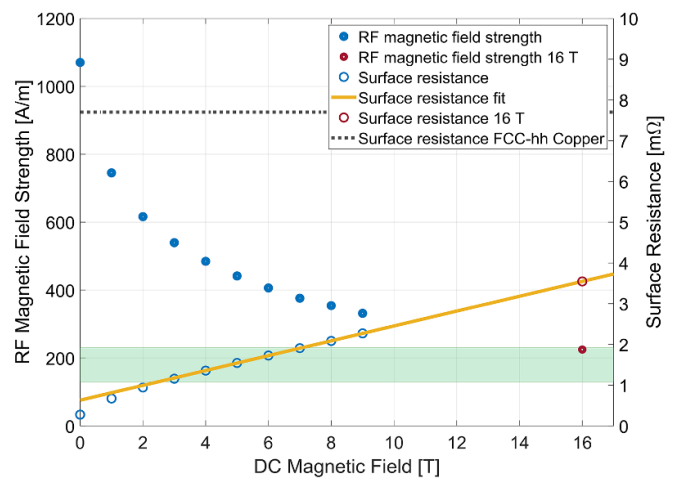


Figure 7. Applied DC magnetic field dependence of the surface resistance R_S and peak RF magnetic field on the samples (H_0) at 50 K. Circles show measured points at B_{DC} from 0 to 9 T. Red circles show extrapolated values for $B_{DC} = 16$ T. The yellow line shows a straight-line fitting following the flux-flow model in [11]. The dashed line indicates the R_S of FCC-hh copper for comparison.

resistance due to lattice defects, grain boundaries, or impurities, and to the BCS contribution described earlier. Using this equation, we extrapolate the value of R_S at 16 T and 8 GHz. Figure 7 shows the fitting and extrapolation for Fujikura APC, which results in $R_S(B_{DC} = 16 \text{ T}; f = 8 \text{ GHz}) = 3.56 \text{ m}\Omega$, less than half that of FCC-hh copper at the same frequency.

Combining equations (4) and (5), we can relate the changes in R_S to the changes in H_0 . This allows us to estimate the value of H_0 at 16 T:

$$H_0 = m_B \sqrt{\frac{P_{diss}(R_S)}{\frac{2}{G} R_S + p \tan(\delta)}}. \quad (8)$$

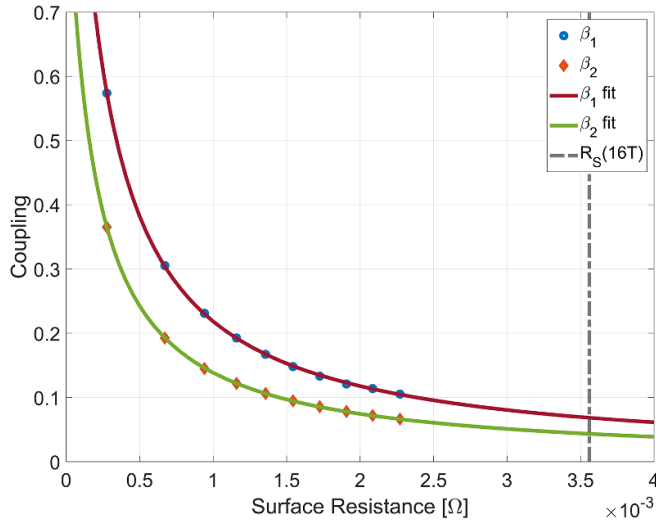


Figure 8. Coupling factors vs. surface resistance in the dielectric resonator with the Fujikura APC sample. Dots are values measured for B_{DC} from 0 to 9 T. Lines are the results of a fitting to $\beta = a/(R_S + b)$, where a and b are the fitting parameters. The vertical line represents the value of R_S for $B_{DC} = 16$ T.

Table 4. Extrapolated surface resistance for all providers at +13 dBm, and their corresponding maximum RF field amplitude. As reference, the values for Cu are $R_S(16$ T, 8 GHz) = 7.8 m Ω and $R_S(16$ T, 1 GHz) = 2.8 m Ω . R_S values at 1 GHz are scaled-down from those at 8 GHz assuming a square dependence of the surface resistance on frequency.

REBCO-CC	H_0 (A m $^{-1}$)	$R_S(16$ T, 8 GHz) (m Ω)	$R_S(16$ T, 1 GHz) ($\mu\Omega$)
Bruker	162	5.3	84.9
Fujikura APC	228	3.7	59.3
SuperPower	207	4.4	70.5
Fujikura	156	4.9	78.5
SuNAM	79	13.0	208.3
SuperOx	109	10.0	160.2
Theva	91	10.3	165.0

In the equation above, we have made explicit the dependence of the power dissipated in the resonator with surface resistance ($P_{diss}(R_S)$) which, in turn, is due to a dependence of the resonator couplings on R_S . As shown in figure 8, coupling factors vary upon changes in R_S . This dependence can be fitted with a rational function $\beta = a/(R_S + b)$, where a and b are the fitting parameters (see details in the supplementary material). Using this function, we can find the values of β_1 and β_2 corresponding to the foreseen value for R_S at $B_{DC} = 16$ T. Using equations (7) and (8), and the extrapolated values of β_1 and β_2 , we can derive the prediction for H_0 at 16 T and 8 GHz as indicated already in figure 7 (red dot). Table 4 summarizes the results for all samples used in this study. Assuming a frequency square dependence of the surface resistance as given by the two-fluid model [39] an extrapolation to 1 GHz has been performed and is also shown in table 4.

Note that, unlike the surface resistance, the peak RF magnetic field strength cannot be extrapolated down to 1 from

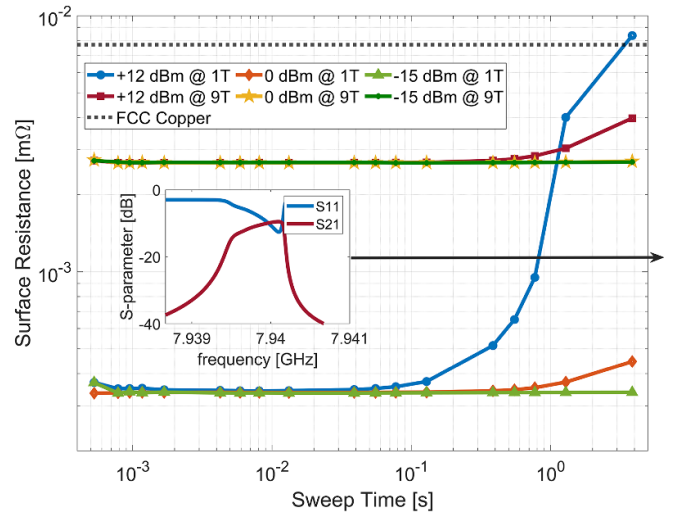


Figure 9. The surface resistance for three different VNA output power at two different applied DC magnetic fields as a function of the sweep time. The only parameter chosen to control the sweep time is the IF bandwidth. The inset figure shows two S-parameters, one reflection and one transmission coefficient, as a function of frequency at resonance. The disturbed resonance curve results for very slow measurements with a sweep time of 15 s. Data is shown for Superpower.

the 8 GHz measurements. This is because the dependence of the coupling factors (β) on R_S (figure 8) is specific of our 8 GHz resonator. Still, the values foreseen for $R_S(16$ T, 1 GHz) are similar to those we reported previously [16] under much weaker RF strength (table 3). Accordingly, our results show that under the working conditions of the FCC-hh, the impact of the H_{RF} power in the $R_S(H_{RF})$ is small and therefore, an RF loss significantly smaller than that attainable with copper is expected with REBCO-CCs even in the presence of the DC and RF fields foreseen in the FCC-hh BS.

5. Transient thermal effects

Measurements of the surface resistance for different VNA output powers as a function of VNA sweep time have been performed for all providers at a stable temperature of 50 K to study possible transient thermal effects [36, 39]. The sweep time has been changed by varying the IF bandwidth. Results for SuperPower are presented in figure 9. It illustrates the surface resistance as a function of VNA sweep time for three different VNA output power (−15, 0, and +13 dBm) at two different applied DC magnetic fields (1 and 9 T). As can be seen in figure 9, the surface resistance asymptotically tends to a constant value for short VNA sweep times. Hence, for fast sweep times there is strong dependence of the surface resistance on the applied DC magnetic field and a minor one on the applied power. VNA power only has a measurable effect for long sweep times. Nevertheless, the onset of sweep time at which the R_S starts increasing and the amplitude of the change depends on the applied DC magnetic field: at 1 T, the sweep time onset is lower than at 9 T, and R_S has a steeper increase at 1 T than at 9 T.

Figure 9 provides indirect information on the thermal time constants in our setup. At frequencies close to resonance, RF fields may heat the samples under measurement. Heat generation is strongest at resonance -at the mid-point of the frequency span- and decays as the VNA frequency departs from resonance. The asymptotic behavior in figure 9 can be explained in terms of VNA sweep time vs. thermal time constant: when the VNA sweep time is much shorter than the thermal time constant, no heat can build up in the samples under measurement. Conversely, when R_S depends on sweep time, we can infer heating effects with time constants comparable to VNA sweep time.

The discussion above can be translated to the FCC-hh by considering that there will be 10 400 circulating bunches in the FCC-hh, each carrying 10^{11} protons with a revolution time of ≈ 0.3 ms. The bunches, separated by 25 ns are assumed to be Gaussian and have an RMS length ($\sigma_t = \sigma_t/c$) of 270 ps [1]. These times are much shorter than the threshold sweep times that affect R_S (figure 8) and suggest that there should not be any transient thermal effects due to the timing structure of the proton beams provided that, as in our setup, the thermal relaxation time constants in the FCC-hh BS are much longer than the length of the proton bunches and the separation between bunches. In [17] it is as well confirmed that in the FCC-hh no thermal issues due to the complex layer of the REBCO-CCs shall develop.

6. Flux shaking

At high magnetic fields, vortex-vortex repulsion forces the vortices to form a lattice in a fine periodic array with highest packing fraction and minimal enthalpy for the arrangement, if possible. In addition, crystal defects, such as vacancies, impurities or dislocations in a material and most recently, artificially created pinning centers, act as traps for vortices. Several studies [40–44] have shown that vortices produced by a DC magnetic field applied perpendicularly to a superconducting surface may be moved by applying a small RF magnetic field that produces an RF sheet current parallel to the surface. This motion (a periodic tilt of the vortex) can be either around the vortex pinning position (fluctuation) or include a net vortex drift (displacement).

When there is no net displacement, vortices have an oscillation motion restricted to their pinning potential well when driven by an applied RF current density [40, 41]. The strength of the Lorentz force exerted on the vortex depends on the pinning force, proportional to the RF current, and the viscous drag exerted during oscillation, which is proportional to the frequency of the RF current. Above the depinning frequency (defined as the ratio of the pinning force to the viscous drag coefficients in the equivalent harmonic oscillator), the viscous forces dominate (flux-flow regime) and the vortex oscillation is strongly dissipative, while at frequencies below the depinning frequency the vortex oscillation is almost nondissipative [45]. Measurements reported in [16] state that the depinning frequencies of all providers are above the resonant frequency

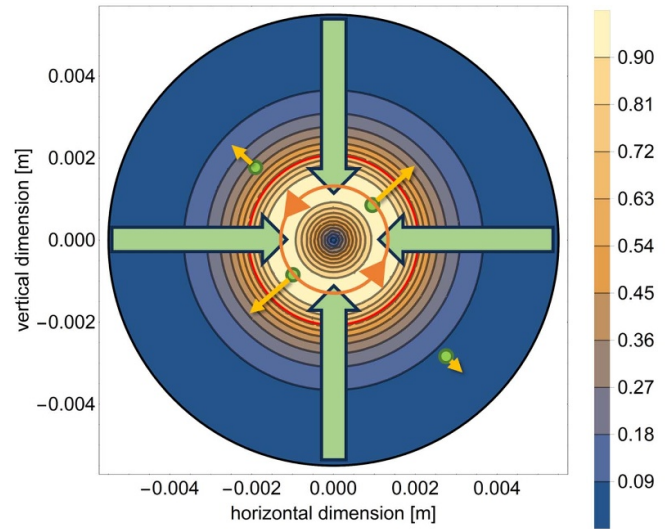


Figure 10. RF surface magnetic field strength distribution H_ρ on a sample ($12 \times 12 \text{ mm}^2$) inside the DR structure. The field strength is normalized to the maximum value. The red line indicates the border of the rutile crystal. The green arrows show the radial $H_\rho(\rho, L)$ distribution, the orange triangles are the resulting azimuthal surface currents at maximum position, the green circles represent vortices at different positions and the overall position-dependent force on them (yellow arrows).

of our measurement and significantly above the FCC-hh mid beam frequency spectrum.

Vortex motion including displacement is normally referred to as vortex shaking effect [42] and explains the generation of a DC electric field due to vortex displacement, which tends to homogenize the overall distribution of the magnetic induction in the critical state. A similar situation occurs in the REBCO-CCs in the FCC-hh BS where the vortices will be subject to a DC magnetic field perpendicular to the RF image currents induced by the beam. This scenario can give rise to a vortex oscillating motion [18] which may include net displacement. Hence, it is essential for the FCC-hh to determine whether the induced RF azimuthal magnetic field strength will be sufficient to fluctuate and/or displace the trapped vortices away from their static position.

These effects can be examined with our dielectric resonator, where vortices are trapped after applying a magnetic field ramp aligned in the axial direction, and they are subject to a single-sided and position-dependent RF-induced radial force following the spatial distribution of H_ρ in figure 10. If RF surface magnetic field strengths are sufficiently strong, the net vortex displacement will move vortices across the sample towards the resonator's axis or the outer rim. In both cases, RF fields are minimal in these areas, so the net displacement of vortices should decrease the RF losses and should result in an increase in quality factor. Therefore, to confirm if the RF magnetic field strength used in this study is sufficient to move vortices after the samples have been magnetized, the following measurement was performed for each provider: First, the REBCO-CC's quality factor was measured at 50 K in

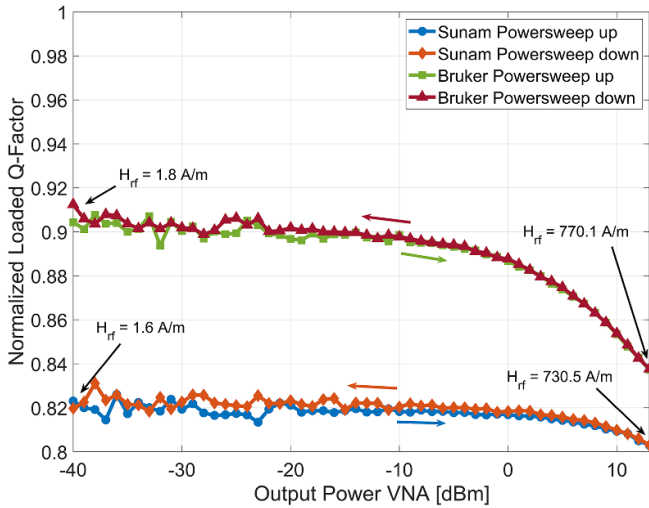


Figure 11. Measured normalized loaded quality factor as a function of the VNA output power for two REBCO-CCs with (Bruker) and without APC (SuNAM). The quality factors are normalized to the 0 T values before the magnetic ramp.

Table 5. Percentage of Q-reduction after exposure to a 9 T magnetic field. Unloaded quality factor measured at -15 dBm VNA output power.

REBCO-CC	(%)
Bruker	10
Fujikura APC	18
SuperPower	5
Fujikura	14
SuNAM	18
SuperOx	6
Theva	10

a zero-field cooled configuration as a function of the VNA output power. Then, the magnetic field is ramped up to 9 T and back to 0 T, leaving the REBCO-CC in a remnant critical state configuration and finally, the quality factor was re-measured as a function of the VNA output power waiting for 10 s per 1 dB. The VNA output power was ramped up and down.

Figure 11 shows the quality factor for two samples (one from Bruker containing APC and a pristine sample from SuNAM) in the remnant critical state relative to their zero-field cooled one. Similar results were obtained for the other samples. The results in figure 11 show that the REBCO-CCs remain in the same critical state after a 9 T ramp, i.e. quality factor does not recover after ramping the VNA output power. Table 5 presents the measured percentage reduction, which is dependent on the provider. A flux shaking mechanism could not be observed on the measurements presented. Only a minor raise (within the sensitivity of the experimental setup) in quality factor is observed for all pristine samples after ramping up and down the RF power, which could indicate a partial vortex displacement of individually weakly pinned vortices but not a complete demagnetization. This is in accordance with [42] that states that a net vortex displacement requires RF

magnetic field amplitudes $H_0 > 0.5 j_C$, where j_C is the critical current per cm-width. If this condition is fulfilled, then the magnetization decreases exponentially. In [13] the measured critical current per cm-width on an equivalent REBCO tape is $j_C \approx 110000 \text{ A m}^{-1}$, which is two orders of magnitude larger than the $H_0 \approx 1200 \text{ A m}^{-1}$ induced on the samples at the maximum VNA output power. This suggests that the vortices fluctuate around their trapped position but have no net displacement, including no influence onto the behavior of the CC, and there is no net increase in quality factor detectable with the dielectric resonator.

7. Conclusion

We have extended our previous study on REBCO-CCs as an alternative FCC-hh BS coating to considerably higher RF power (a factor 630 with respect to our previous measurements), including exposure to RF fields comparable or (often) higher than those expected in the BS of the FCC-hh. We show that the performance of a REBCO-CC-coating in a particle accelerator is not only affected by the DC magnetic field but also by the RF fields induced by the image currents flowing in the BS due to the temporal structure of the proton beam. Seven different REBCO-CC samples have been investigated under DC and RF magnetic fields at 50 K and 8 GHz using a rutile loaded dielectric resonator. A DC magnetic field up to 9 T was applied perpendicular to the samples, and at the same time, RF magnetic fields up to 1.4 mT were applied perpendicularly to the DC field. We have numerically calculated the actual FCC-hh baseline BS expected RF azimuthal magnetic field strength and compared it with RF magnetic field strengths generated in the dielectric resonator. We have proven that we can measure above or within FCC-hh RF magnetic field strengths conditions up to 9 T. The results show that at 8 GHz and depending on the microstructure, not all REBCO-CCs outperform copper at 9 T. However, when the results are extrapolated to FCC-hh conditions (1 GHz, 16 T), all REBCO-CCs studied should outperform Cu by one or two orders of magnitude. Further, the measurements revealed that the results at such high output power depend as well on the VNA sweep time. We have discussed the correlation between the electromagnetic fields provided by the VAA and the timing of the circulating proton bunches, proving that the onset for thermal effects starts at times much larger than the characteristic timings of the circulating proton bunches, and therefore, transient thermal effects in the BS shall not affect the surface resistance of REBCO-CCs. We did not find improvements in the quality factor of samples in the remnant state after ramping the VNA power, indicating no net flux displacement caused by applying RF magnetic field to the samples. This happened for samples containing APC as well as for pristine samples. In all, we have demonstrated that, despite the dependence of REBCO-CC's surface resistance on DC and RF magnetic fields, these materials can significantly lower the surface resistance of the FCC-hh BS coating, and with that, the beam impedance.

Data availability statement

All data that support the findings of this study are included within the article (and any supplementary files).

Acknowledgments

The authors acknowledge the support and samples provided by Bruker HTS GmbH, Fujikura Ltd, SuNAM CO Ltd SuperOx, SuperPower Inc. and Theva Dünnschichttechnik GmbH. This work was supported by CERN under Grant Nos. FCC-GOV-CC-0072/KE3358, FCC-GOV-CC-0153/KE4106 and FCC-GOV-CC-0208/KE4947/ATS. UPC funding was also provided through the Unit of Excellence María de Maeztu MDM2016-0600. N Tagdulang and A Romanov acknowledge MSCA-COFUND-2016-754397 for the PhD Grant. ICMAB authors acknowledge RTI2018-095853-B-C21 SuMaTe from MICINN and co-financing by the European Regional Development Fund; 2017-SGR 1519 from Generalitat de Catalunya and COST Action NANOCO-HYBRI (CA16218) from EU, the Center of Excellence award Severo Ochoa CEX2019-000917-S.

ORCID iDs

P Krkotić  <https://orcid.org/0000-0003-1892-0350>
 N Tagdulang  <https://orcid.org/0000-0002-6248-0906>
 G Telles  <https://orcid.org/0000-0002-2620-7283>
 J Gutierrez  <https://orcid.org/0000-0002-8897-0276>
 S Calatroni  <https://orcid.org/0000-0002-2769-8029>
 M Pont  <https://orcid.org/0000-0003-4830-2692>
 J M O'Callaghan  <https://orcid.org/0000-0002-2740-0202>

References

- [1] Benedikt M et al 2019 *Eur. Phys. J. Spec. Top.* **228** 755–1107
- [2] Brüning O S, Collier P, Lebrun P, Myers S, Ostojic R, Poole J and Proudlock P 2004 *LHC Design Report (Cern Yellow Reports: Monographs)* (Geneva: CERN)
- [3] Bellafont I, Mether L, Kersevan R, Malyshev O, Baglin V, Chiggiato P and Pérez F 2020 *Phys. Rev. Accel. Beams* **23** 043201
- [4] Lebrun P and Taviani L 2015 *25th Int. Cryogenic Conf. and Int. Cryogenic Conf.*
- [5] Bellafont I, Morrone M, Mether L, Fernández J, Kersevan R, Garion C, Baglin V, Chiggiato P and Pérez F 2020 *Phys. Rev. Accel. Beams* **23** 033201
- [6] Arsenyev S, Boine-Frankenheim O and Schulte D 2018 *Proc. 9th Int. Particle Conf. (IPAC'18)*
- [7] Astapovych D, Boine-Frankenheim O, Gubaidulin V, Kornilov V, Niedermayer U and Schulte D 2021 *J. Instrum.* **16** 01013
- [8] Hein M 1999 *High-Temperature-Superconductor Thin Films at Microwave Frequencies* (Heidelberg: Springer)
- [9] Calatroni S 2016 *IEEE Trans. Appl. Supercond.* **26** 3500204
- [10] Calatroni S and Vaglio R 2017 *IEEE Trans. Appl. Supercond.* **27** 3500506
- [11] Calatroni S, Bellingeri E, Ferdeghini C, Putti M, Vaglio R, Baumgartner T and Eisterer M 2017 *Supercond. Sci. Technol.* **30** 075002
- [12] Krkotić P, Niedermayer U and Boine-Frankenheim O 2018 *Nucl. Instrum. Methods Phys. Res. A* **895** 56–61
- [13] Puig T et al 2019 *Supercond. Sci. Technol.* **32** 094006
- [14] Vaglio R and Calatroni S 2019 *Eur. Phys. J. Spec. Top.* **228** 749–54
- [15] Patsch S, Niedermayer U, Stem W D and Boine-Frankenheim O 2019 *IEEE Trans. Appl. Supercond.* **29** 8200810
- [16] Romanov A et al 2020 *Sci. Rep.* **10** 12325
- [17] Vaglio R and Calatroni S 2019 *Eur. Phys. J. Spec. Top.* **228** 749–54
- [18] Calatroni S and Vaglio R 2021 *IEEE Trans. Appl. Supercond.* **31** 3500208
- [19] Powell J R, Porch A, Kharel A P, Lancaster M J, Humphreys R G, Wellhöfer F and Gough C E 1999 *J. Appl. Phys.* **86** 2137–45
- [20] Seron D, Collado C, Mateu J and O'Callaghan J 2006 *IEEE Trans. Microw. Theory Tech.* **54** 1154–60
- [21] Collado C, Mateu J and O'Callaghan J 2005 *IEEE Trans. Appl. Supercond.* **15** 26–39
- [22] Mateu J, Collado C, Menéndez O and O'Callaghan J M 2003 *App. Phys. Lett.* **82** 97–99
- [23] Mateu J, Collado C, Menéndez O and O'Callaghan J M 2003 *J. Supercond. Novel Magn.* **16** 873–80
- [24] Mateu J, Collado C, Orloff N, Booth J, Rocas E, Padilla A and O'Callaghan J 2009 *IEEE Trans. Microw. Theory Tech.* **57** 10–18
- [25] Collado C, Mateu J and O'Callaghan J 2001 *IEEE Trans. Appl. Supercond.* **11** 1396–9
- [26] Hakki B and Coleman P 1960 *IEEE Trans. Microw. Theory Tech* **8** 402–10
- [27] Klein N, Zuccaro C, Dähne U, Schulz H, Tellmann N, Kutzner R, Zaitsev A G and Wördenweber R 1995 *J. Appl. Phys.* **78** 6683–6
- [28] Shen Z Y, Wilker C, Pang P, Holstein W, Face D and Kountz D 1992 *IEEE Trans. Microw. Theory Tech* **40** 2424–31
- [29] Mazierska J and Grabovickic R 1998 *IEEE Trans. Appl. Supercond.* **8** 178–87
- [30] Wosik J, Krupka J, Qin K, Ketharnath D, Galstyan E and Selvamaniackam V 2017 *Supercond. Sci. Technol.* **30** 035009
- [31] Lee S Y, Lee J H and Jung H S 2009 *J. Korean Phy. Soc.* **54** 1619–25
- [32] Kajfez D and Guillon P 1986 *Dielectric Resonators* (Norwood: Artech House)
- [33] Krkotić P, Aguasca A and O'Callaghan J M 2018 *48th European Conf. (EuMC)*
- [34] Krkotić P, Gallardo Q, Tagdulang N D, Pont M and O'Callaghan J M 2021 *IEEE Trans. Microw. Theory Tech.* **69** 3917–26
- [35] Ginzton E L 1957 *Microwave Measurements* (New York: McGraw-Hill)
- [36] Rabinowitz M 1970 *Lett. Nuovo Cimento* **4** 549–53
- [37] Pozar D M 2005 *Microwave Engineering* 3rd edn (Hoboken, NJ: Wiley)
- [38] Coffey M W and Clem J R 1992 *Phys. Rev. B* **45** 10527–35
- [39] Prozorov R, Giannetta R W, Carrington A, Fournier P, Greene R L, Guptasarma P, Hinks D G and Banks A R 2000 *App. Phys. Lett.* **77** 4202–4
- [40] Coffey M W and Clem J R 1991 *Phys. Rev. Lett.* **67** 386–9
- [41] Gittleman J I and Rosenblum B 1968 *J. Appl. Phys.* **39** 2617
- [42] Brandt E H and Mikitik G P 2002 *Phys. Rev. Lett.* **89** 027002
- [43] Mikitik G P and Brandt E H 2003 *Phys. Rev. B* **67** 104511
- [44] Brandt E H and Mikitik G P 2007 *Supercond. Sci. Technol.* **20** S111–6
- [45] Golosovsky M, Tsindlekht M, Chayet H and Davidov D 1994 *Phys. Rev. B* **50** 470–7